Two-Dimensional LTE Modeling of a Low-Power Argon Arcjet Thruster

IEPC-2009-258

Presented at the 31st International Electric Propulsion Conference,

University of Michigan • Ann Arbor, Michigan • USA

September 20 – 24, 2009

Hai-Xing Wang[1]， Shao-Xia Jia[2]

Beijing University of Aeronautics and Astronautics, Beijing, 100191, China

Xi Chen[3]

Tsinghua University, Beijing, 100084, China

and

Wenxia Pan[4]

Institute of Mechanics, Chinese Academy of Sciences, Beijing, 100190

Abstract：The extension to a higher specific impulse of an arcjet requires deeper understanding of the physics process in the thruster. In this paper, low-power arcjet thrusters are studied numerically using argon as the propellant. The all-speed SIMPLE algorithm is used for the solution of the governing equations, including temperature- and pressure-dependent gas properties. Computed results are presented concerning the temperature, pressure, axial velocity and Mach number distributions within in the thruster nozzle under typical operating conditions. It is found that the heating of the propellant takes place mainly in the constrictor. Under typical operating conditions studied here, the computed specific impulses and mass flow rates of the argon arcjet thruster are roughly consistent with corresponding experimental data. The effects of the geometrical sizes of the arcjet are also investigated.

Nomenclature

A = cathode end area

B_θ = magnetic induction intensity

C_p = specific heat at constant pressure

e = elementary charge

F = thrust

G = mass flow rate

g = gravitational acceleration

[1] Associate Professor, School of Astronautics, whx@buaa.edu.cn

[2] Graduate Student, School of Astronautics, jiashaoxi@163.com

[3] Professor, Department of Engineering Mechanics, cx-dem@tsinghua.edu.cn

[4] Professor, wxpan@imech.ac.cn

h = specific enthalpy
I = arc current
I_{sp} = specific impulse
j = current density
k_B = Boltzmann constant
$\dot{m}$ = the mass flow rate
p = gas static pressure
R = gas constant
T = gas temperature
U_r = radiation power per unit volume of plasma
u = axial velocity
$\mathbf{V}$ = the velocity vector
v = radial velocity
γ = specific-heat ratio
κ = thermal conductivity
μ = viscosity
μ_0 = the magnetic permeability
ρ = gas density
σ = electric conductivity
σ_c = the electric conductivity of cathode material
ϕ = electrical potential
Φ = viscous dissipation

I. Introduction

Arcjet thruster is an electrothermal propulsion device in which gaseous propellant is heated by means of a high temperature DC arc. The arc emanates from the cathode, passes through a constrictor, and attaches on the nozzle-anode wall. The gaseous propellant is injected from the upstream end of arcjet and heated to a high temperature with order of 10^4 K , then expands through a convergent-divergent nozzle to convert the thermal energy into the kinetic energy and thereby produces a thrust. Due to their high specific impluse, long service life and economic advantages, low-power arcjet systems have now been used for north-south station keeping on commercial satellites. The next step for the arcjet technology advance will extend to orbit transfer missions using high power arcjets and explore the possibility of employing other propellants.

Typical low-power arcjets (0.5 to 2.0 kW) have conical converging-diverging nozzles with constrictor diameters on the order of 0.5−0.6 mm, nominal expansion angles of ~20°. The physical characteristics of the arcjet flow field vary from highly ionized plasma at temperatures in excess of 15000 K near the cathode tip to a few thousands K at the thruster exit. Velocities vary from several km/s on the nozzle centerline to zero at the nozzle wall. Considering the large radial change of these plasma parameters and the small geometric length, it is clear that the physical processes in the arcjet are very complex. Although a lot of experimental and modeling results concerning the arcjet thruster performance and characteristics have been accumulated in the literature[1,2], some important physical processes which govern the performance of an arcjet are still poorly understood.

Recently, expermental arcjet systems have been established at the School of Astronautics of Beijing Univeristy of Aeronautics and Astronautics(BUAA)[3] and at the Institute of Mechanics of the Chinese Academy of Sciences[4] and a series of experimental results have been obtained about the arcjet thruster characteristics.

Modeling study is thus conducted in order to understand the heat transfer and fluid flow processes within the arcjet thruster and to provide preliminary estimates of the thruster performance. The modeling approach and typical modeling rusults are presented and followed by conclusions.

II. Modeling approach

Figure 1 is a schematic diagram of the low-power argon arcjet thruster under study with geometrical sizes almost the same as those used in the experimental investigations of BUAA and this thruster will be called Nozzle I arcjet in the following sections. The consitctor of the Nozzle I arcjet is 0.5 mm long with a diameter of d=0.7 mm. Because of the axisymmetry of fluid flow within the arcjet nozzle, only the upper half of the arcjet thruster is taken as the computational domain. Altogether 74 (z-direction) ×21 (r-direction) grid points are employed in this modeling study.

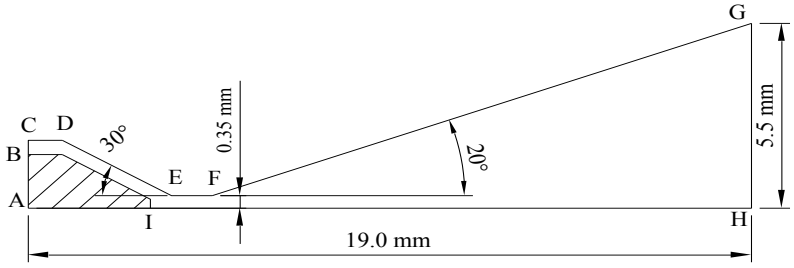

Figure 1. Schematic diagram of the low-power arcjet thruster

The main assumptions employed in this study are as follows. (1) The plasma flow in the arcjet is steady, axisymmetrical, laminar and compressible; (2) the plasma is optically thin and in the LTE state; (3) the swirling velocity component is negligible in comparison with the axial velocity.

Based on the foregoing assumptions, the governing equations in cylindrical coordinates (r, z) can be written as follows[5, 6].

$$\frac{\partial}{\partial z}(\rho u)+\frac{1}{r}\frac{\partial}{\partial r}(r\rho v)=0 \tag{1}$$

$$\frac{\partial(\rho uu)}{\partial z}+\frac{1}{r}\frac{\partial(r\rho uv)}{\partial r}=-\frac{\partial p}{\partial z}+2\frac{\partial}{\partial z}\left(\mu\frac{\partial u}{\partial z}\right)+\frac{1}{r}\frac{\partial}{\partial r}\left[r\mu\left(\frac{\partial u}{\partial r}+\frac{\partial v}{\partial z}\right)\right]+j_r B_\theta \tag{2}$$

$$\frac{\partial(\rho uv)}{\partial z}+\frac{1}{r}\frac{\partial(r\rho vv)}{\partial r}=-\frac{\partial p}{\partial r}+\frac{2}{r}\frac{\partial}{\partial r}\left(r\mu\frac{\partial v}{\partial r}\right)+\frac{\partial}{\partial z}\left[\mu\left(\frac{\partial v}{\partial z}+\frac{\partial u}{\partial r}\right)\right]-2\mu\frac{v}{r^2}-j_z B_\theta \tag{3}$$

$$\begin{aligned}\frac{\partial(\rho uh)}{\partial z}+\frac{1}{r}\frac{\partial(\rho rvh)}{\partial r}&=\frac{\partial}{\partial z}\left(\frac{\kappa}{c_P}\frac{\partial h}{\partial z}\right)+\frac{1}{r}\frac{\partial}{\partial r}\left(r\frac{\kappa}{c_P}\frac{\partial h}{\partial r}\right)+u\frac{\partial p}{\partial z}+v\frac{\partial p}{\partial r}\\&+\Phi-\frac{2}{3}\mu(\nabla\cdot\boldsymbol{V})^2+\frac{j_z^2+j_r^2}{\sigma}+\frac{5k_B}{2e}\left(\frac{j_z}{c_P}\frac{\partial h}{\partial z}+\frac{j_r}{c_P}\frac{\partial h}{\partial r}\right)-U_r\end{aligned} \tag{4}$$

The electrical potential ϕ is solved by

$$\frac{1}{r}\frac{\partial}{\partial r}\left(r\sigma\frac{\partial\phi}{\partial r}\right)+\frac{\partial}{\partial z}\left(\sigma\frac{\partial\phi}{\partial z}\right)=0 \tag{5}$$

The viscosity disspation term in Eq.(4) is calculated by

$$\Phi = \mu\left\{2\left[\left(\frac{\partial v}{\partial r}\right)^2 + \left(\frac{v}{r}\right)^2 + \left(\frac{\partial u}{\partial z}\right)^2\right] + \left(\frac{\partial v}{\partial z} + \frac{\partial u}{\partial r}\right)^2\right\} \tag{6}$$

The current density components j_r and j_z in Eqs.(2)−(4) and the self-induced magnetic induction intensity B_θ are calculated by

$$j_r = -\sigma\frac{\partial \phi}{\partial r} \qquad j_z = -\sigma\frac{\partial \phi}{\partial z} \qquad B_\theta = \frac{\mu_0}{r}\int_0^r j_z \xi d\xi \tag{7}$$

The adopted boundary conditions are as follows. At the inlet section of the arcjet nozzle, the gas temperature is given to be 500 K while the stagnant pressure p_0 is taken to be 2.5 atm. The inflowing gas flow is assumed to be uniform and parallel to the thurster wall, and the axial velocity component u is calculated from the stagnat pressure and the local static pressure and temperature using the isentropic compressible flow relation

$$\left(\frac{p_0}{p}\right)^{(\gamma-1)/\gamma} = 1 + \left(\frac{\gamma-1}{2}\right)\frac{u^2}{\gamma RT} \tag{8}$$

The incoming gas flow rate is determined by the iteration precess itself[5]. The temperature along the anode inner-surface is set to increase linearly from 500 K at the nozzle inlet to 1800 K at the end of the constrictor, and then decrease linearly to 700 K at the nozzle exit. At all solid boundaries of the arcjet, zero velocity components are employed. Axi-symmetrical conditions are used at the arcjet axis, whereas the temperatures and velocities at the outlet section of the arcjet are evaluated by extrapolation. At the rear end of cathode (A-B in Fig.1), $\partial\phi/\partial z = I/(A\sigma_c)$ are used. $\phi = 0$ is set along the inner surface of the divergent nozzle after the constrictor (F-G in Fig. 1).

The governing equations are solved using the computer program[5], which is a version of the FAST-2D program[7] modified to include variable gas properties and compressible effects. An all-speed SIMPLE algorithm has been incorporated into the FAST-2D program to simulate the present subsonic–supersonic flow in the thruster nozzle. The governing equations (1) – (5) are solved using the modified FAST-2D program with the auxiliary relations (6) – (8) and the specified boundary conditions to obtain the velocity, pressure and specific enthalpy (or temperature) distributions within the whole thruster nozzle. Mass conservation is ensured in the computation, *i.e.* the axial gas mass flux is constant for all the cross sections of the nozzle.

III. Results and discussion

A. Modeling results of the Nozzle I arcjet

Typical modeling results for the Nozzle I arcjet thruster are presented in Figs.2−6 with different arc

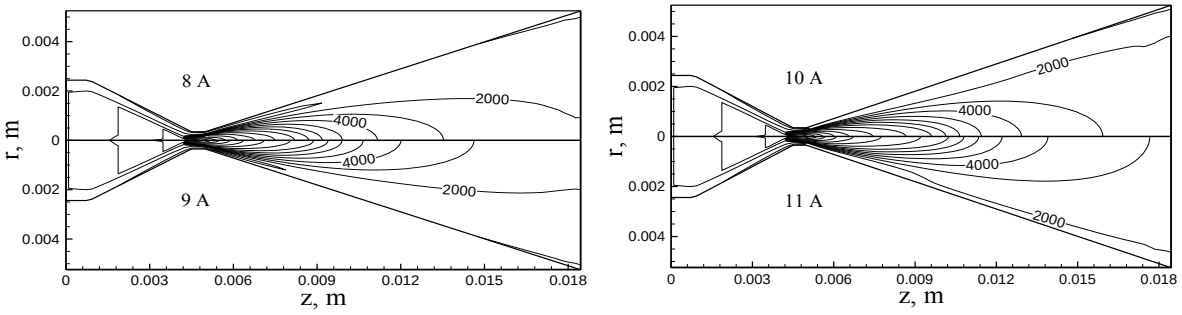

Figure 2. Computed temperature distribution within the arcjet (unit: K, interval 1000 K)

currents (8, 9, 10 and 11 A) but a fixed inlet stagnant pressure (2.5 atm). It is seen from Fig. 2 that the gaseous propellant entering the thruster at temperature 500 K assumes rapid temperature rise due to the Joule heating. The heating of the propellant takes place mainly in the constrictor region and the highest temperature appears at the location near the cathode tip where the current density assumes its maximum value. In the diverging part of the nozzle, the gas temperature decreases gradually because the thermodynamic expansion becomes more dominant than the Joule heating. Gas temperatures are seen to increase with the increase of the arc current.

Figure 3 and Fig. 4 present the plasma axial-velocity and Mach number distributions within the arcjet. The flow transits from subsonic to supersonic within the constrictor and the flows can be approximately divided into three regions, *i.e.* the subsonic regime at the inlet section, the transonic regime in the constrictor, and the supersonic regime in the diverging nozzle. Figure 5 shows that most of the incoming propellant flow rate concentrates in the outer region near the nozzle wall.

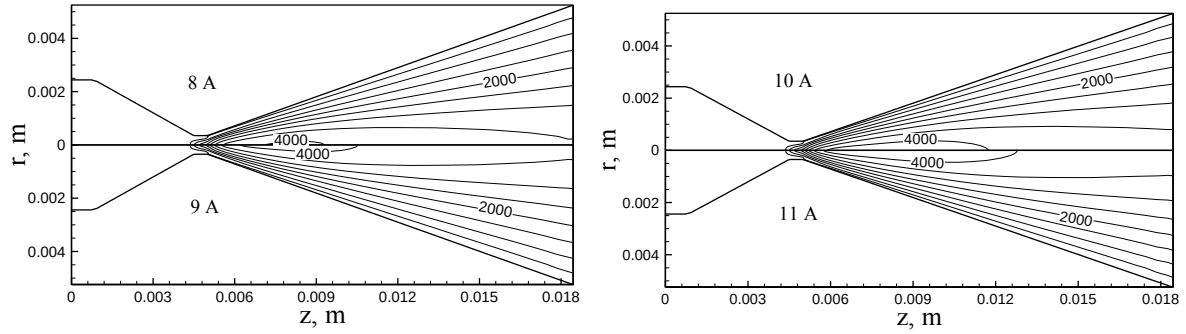

Figure 3. Computed axial velocity distribution within the arcjet (unit: m/s, interval 500 m/s)

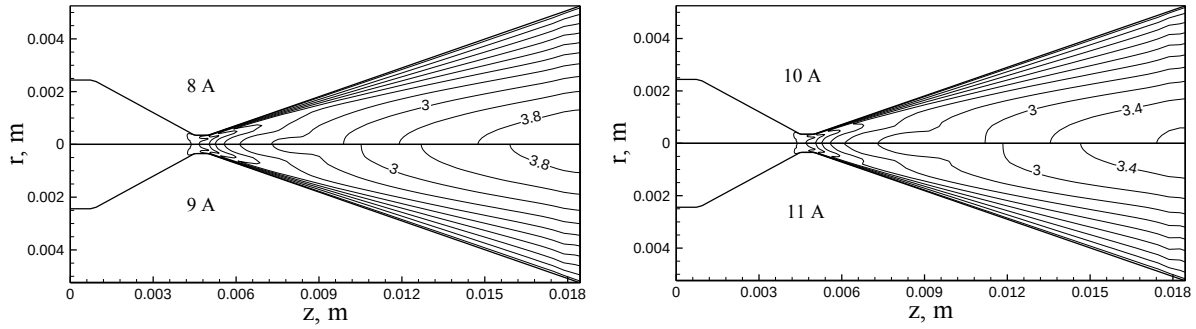

Figure 4. Computed Mach number distribution within the arcjet (interval 0.4)

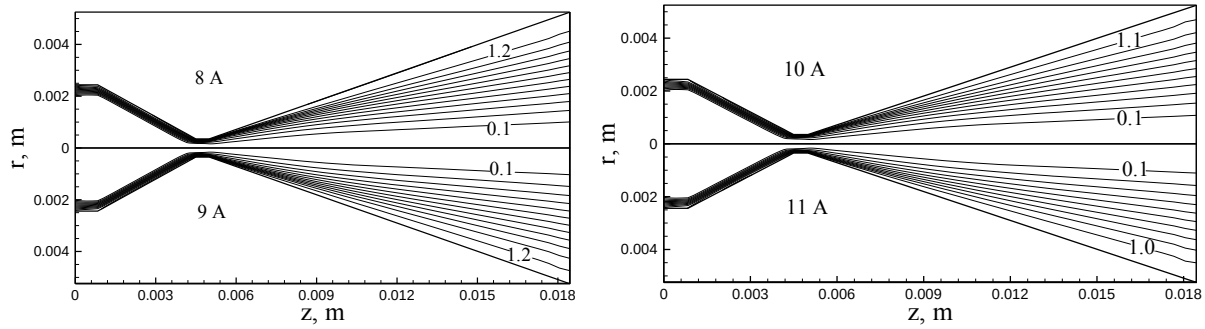

Figure 5. Computed streamlines within the arcjet (interval 1.0×10^{-6} kg/s)

Figure 6 a) and b) present the plasma axial-velocity and temperature profiles along the nozzle axis for the cases with fixed inlet stagnant pressure 2.5 atm but with four different arc currents (*i.e.* 8 , 9, 10 and 11 A). It is seen that the maximum axial-velocities are 4042 m/s, 4137 m/s, 4248 m/s and 4361 m/s correspongding to the

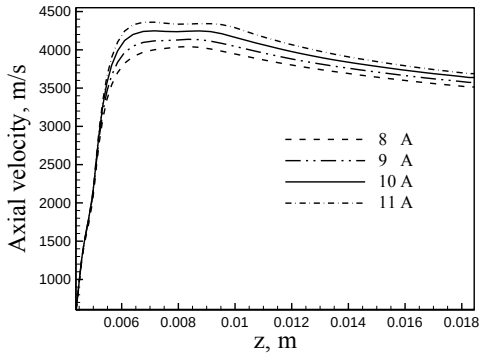

a) Axial-velocity distribution

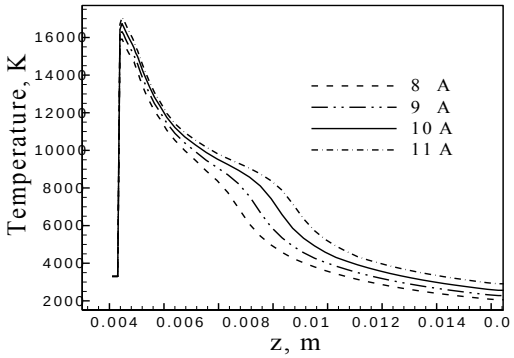

b) Temperature distributions distribution

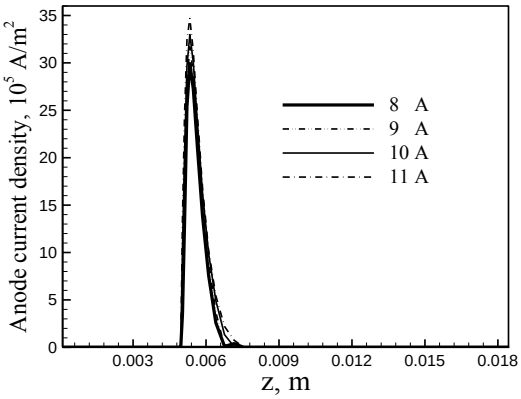

c) Current density distribution

Figure 6. Comparison of the plasma axial-velocity a), temperature b) along the thruster nozzle axis, and current density along the anode surface c)

arc currents of 8 A, 9 A, 10 A and 11 A. At the outlet of the arcjet thruster, the axial velocities decrease to 3514 m/s, 3574 m/s, 3638 m/s and 3689 m/s, respectively. It is also seen that correspongding to the arc currents of 8 A, 9 A, 10 A and 11 A, the peak temperatures are 15920 K, 16310 K, 16740 K and 17070 K which appear at approximately z= 4.5 mm, *i.e.* near the cathode tip. Then the plasma temperatures decrease gradually along the nozzle axis as the plasma flows towards the thrust exit. At the exit of the arcjet, the predicited temperature at centerline of thruster are 2057 K, 2281 K, 2562 K and 2907 K, respectively. Fig. 6 c) shows the current density distri butions along the anode surface. It is noted the maximum current densities at the anode attachment region are 3.0×10^6 A/m^2, 3.2×10^6 A/m^2, 3.3×10^6 A/m^2 and 3.5×10^6 A/m^2, respectively, correspongly to the arc currents of 8 A, 9 A, 10 A and 11 A, and the peak values of current density appear at the location roughly 0.5 mm downstream from the constrictor.

The computed radial profiles of the axial velocities, Mach numbers, static pressures, and temperature for the cases with fixed inlet stagnant pressure 2.5 atm and four different arc currents (*i.e.* 8 , 9, 10 and 11 A) at the exit of the nozzle are plotted in Fig.7. Figure 7 a) shows that the predicted maximum axial-velocity at the exit plane are 3514 m/s, 3574 m/s, 3638 m/s and 3689 m/s, respectively. Figure 7 b) and c) show that the predicted highest Mach number are 4.16, 4.02, 3.86 and 3.67, whereas the the static pressure are 245 Pa, 253 Pa, 256 Pa and 271 Pa for the arc currents of 8 A, 9 A, 10 A and 11 A, respectively. The highest plasma temperatures appear at the center of the thruster exit, as seen in Fig. 7 d).

As mentioned above, in this study the inlet gas velocity is calculated by Eq. (8) from the given stagnant pressure and the local static pressure and temperature, instead of from a given gas flow rate. After convergent

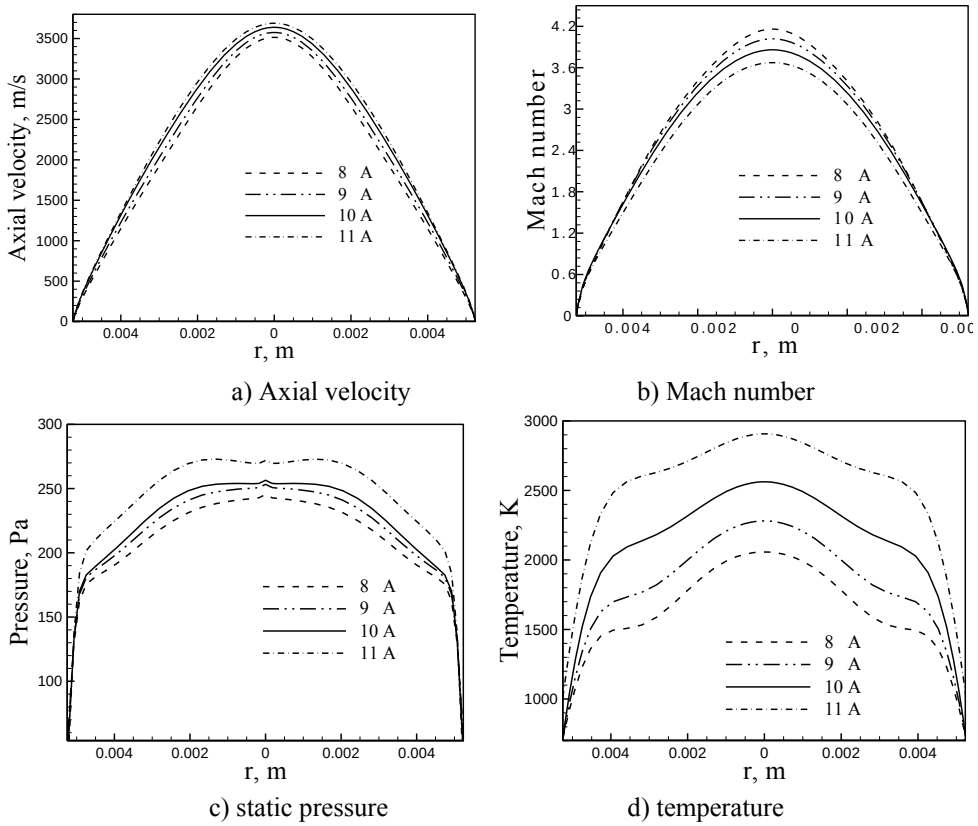

Figure 7. Comparision of the outlet parameters with different currents

solution has been obtained, employing the computed results of gas density ρ and axial velocity u at the thrusterexit section, the mass flow rate G can be calculated by $G = \int_0^{r_0} (\rho u) 2\pi r dr$, while the specific impulse I_{sp} of the arcjet thruster (defined as the thrust force per unit weight flow-rate of propellant) is calculated by $I_{sp} = F/(Gg) = \int_0^{r_0} (\rho u^2) 2\pi r dr/(Gg)$. In the present modeling, the computed argon mass flow rates are are 81.3 mg/s, 78.7 mg/s, 72.8 mg/s and 68.2 mg/s for arc currents of 8 A, 9 A, 10 A and 11 A, respectively. Correspondingly, the computed specific impulses are 205 s, 213 s, 223 s and 230 s, respectively. These computed values of the mass flow rate and the specific impulse of the argon arcjet thruster are roughly consistent with our experimental measured results.

B. Comparsion of modeling results with two types of arcjet

In this study, modeling is also performed for a arcjet with different geometrical sizes from Nozzle I arcjet and this arcjet will be called Nozzle II arcjet in the following. The Nozzle II arcjet consitrictor is 1 mm long with a diameter of d=0.7 mm, while the consitctor of the Nozzle I arcjet studied in the previous section is 0.5 mm long with a diameter of d=0.7 mm. The diverging half-angle and area ratio of the Nozzle II arcjet are 15° and 200, whereas that of the Nozzle I arcjet are 20° and 225, respectively. In order to compare the heat transfer and plasma flow characteristicts in these two arcjet thruster, almost the same operating conditions are adopted in our modeling, *i.e.* the inlet stagnant pressure of the Nozzle II arcjet are also set to be 2.5 atm and the arc currents are taken to be 8 A, 9 A, 10 A 11 A, respectively.

Figures 8 and 9 compare the computed distributions of isotherms and Mach number within the nozzle II arcjet thruster for different arc currents in the range of 8 – 11 A. Similar to the cases of Nozzle I arcjet shown in

Fig. 2 – 5 , Joule heating is still found to be the important source of energy for the regions near the cathode and the in the constrictor.

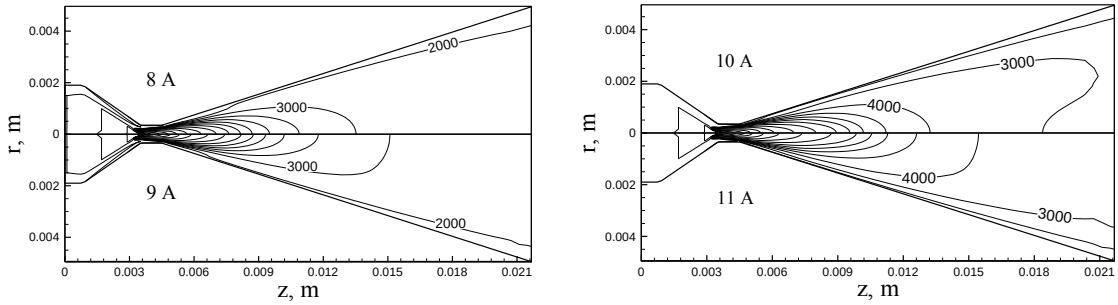

Figure 8. Computed temperature distributions within the arcjet (unit: K, interval 1000 K)

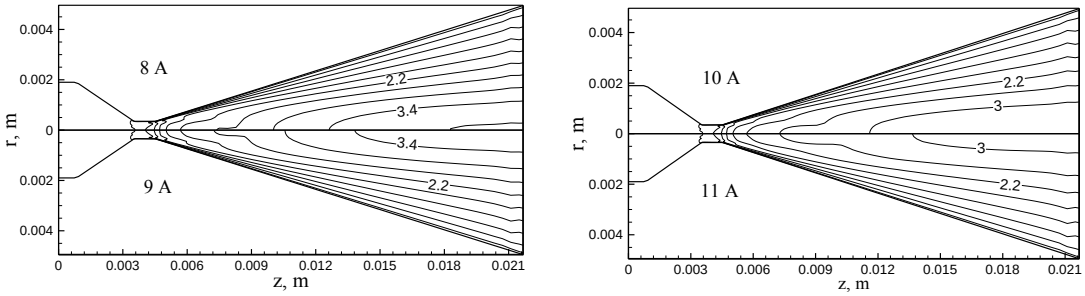

Figure 9. The Mach number distributions in the Nozzle II arcjet

Figure 10 compares the axial variations of the plasma temperature and the axial velocity for the two types of arcjets. Overall, the axial variation plasma temperature and velocity in the two arcjets are very similar. Due to the difference of the constrcitor length, the values and locations of the centerline maximum temperature and axial -velocity are somewhat different. The centerline maximum temperature and axial veolcity are 19970 K and 4119 m/s in the Nozzle II arcjet, while in the the Nozzle I arcjet, the centerline maximum temperature and axial velocity are 16740 K and 4248 m/s if the stagnant pressure is fixed to be 2.5 atm.

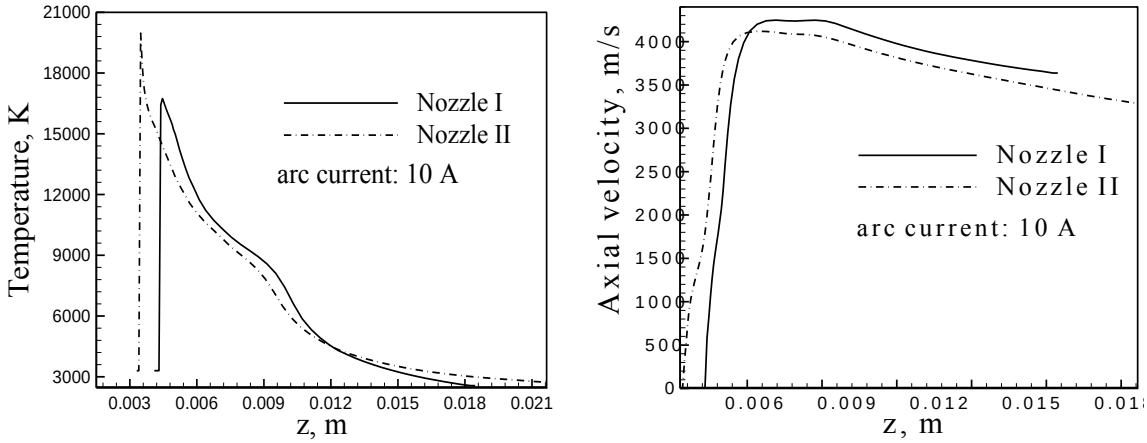

a) temperature b) axial velocity

Figure 10. Comparison of the temperature a), plasma axial-velocity b) along the thruster nozzle axis

Figure 11 compares the computed radial profiles of the plasma temperature and Mach number at the thruster exit plane for the two types of arcjets. It is noted that radial profiles of plasma temperature at the exit plane are different for the two arcjets, as shown in Fig. 11 a). The temperature profiles at the exit plane exhibit

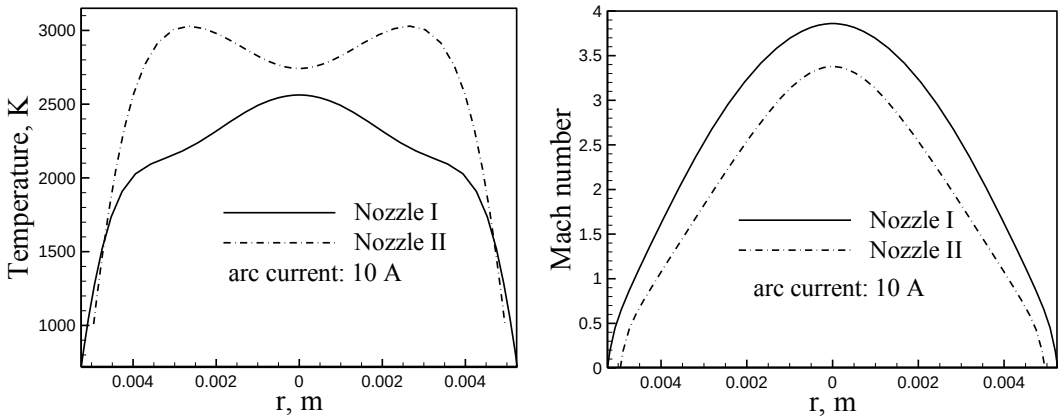

a) temperature b) Mach number

Figure 11. Radial distributions of the temperature at the exit plane (arc current: 10 A)

a bulge near the anode of Nozzle II arcjet. This very noticeable buldge in the temperature profiles is reminiscent of hypersonic thermal boundary layers near cooled surfaces, and is also observed by Aithal *et al* on a hydrogen arcjet[8,9]. The cause of the local maximum in the temperature profile is perhaps due to the opposing effects of flow stagnation and viscous dissipation heating and the relatively colder wall trying to cool the flow. In some results of DSMC calculations[10,11], the temperature profiles at the thrust exit also display such a bulge. A quite different temperature profile at the exit plane of Nozzle II arcjet from Nozzle I is also shown here in Fig. 11 a), *i.e*. the highest plasma temperature for the Nozzle II arcjet does not appear at the center of the thruster exit. In this temperature profile, the plasma temperature does not decrease non-monotonously from the centerline to the nozzle wall. Such a non-monotonous temperature profile was observed by Walker[12] in the experimental studies on a helium arcjet thrusters and the non-monotonous temperature profile was called "U-shape" distribution in Ref. [12]. The characteristic U-shape in the temperature profile implies that the plasma at the thruster central region expands to a temperature somewhat lower than that in the outer region, where the gas temperature is appreciably higher than the nozzle-wall temperature. As seen in Fig. 11 b), the pedicted highest Mach number of the Nozzle I arcjet is 3.86 and it is slightly higher than 3.40 of the Nozzle II arcjet. The predicted mass flow rates and specific impulse are 72.8 mg/s and 223 s, respectively, for the Nozzle I arcjet with arc current of 10 A, while the corresponding mass flow rates and specific impulse of Nozzle II arcjet are 46.3 mg/s and 205 s, respectively.

Non-LTE effects and plasma sheaths at the cathode and anode surfaces are not included in the present preliminary modeling study, although they certainly affect the plasma flow and heat transfer in the subsonic-supersonic thruster nozzle. A more comprehensive modeling approach should include all those complicated factors, although so far it is still a highly challenging task. This would be the subject of further studies.

IV. Conclusions

Modeling results are presented for the plasma flow and heat transfer characteristics of the low-power argon arcjet thruster. The effects of main operating parameters, *i.e*. the arc current, and the geometrical sizes on the plasma flow and heat transfer characteristics have been examined in some details. Modeling results show that the maximum plasma temperature appears in the upstream region of the nozzle near the cathode; the maximum plasma axial-velocity appears near the downstream end of the constrictor; the flow within the thruster nozzle can be divided into three distinctive regions characterized by subsonic, transonic, and supersonic flow regimes,

respectively. The computed mass flow rates and specific impulses of arcjet thruster are roughly consistent with corresponding experimentally measured values. It is revealed that the geometrical configuration affects appreciably the plasma flow and heat transfer characteristics of the arcjets.

Acknowledgments

This work was supported by the National Natural Science Foundation of China (Nos. 50836007，10621202).

References

[1] Martinez-Sanchez M., Miller S. A., "Arcjet modeling: status and prospects", Journal of Propulsion and Power, Vol. 12, No. 6, 1996, pp. 1035-1043

[2] Auweter-Kurtz M, Glocker B, Goelz T, etc. "Arcjet thruster development", Journal of Propulsion and Power, Vol. 12, No. 6, 1996, pp. 1007-1083

[3] Zhang X. A., Tang H. B., Liu Y., et al., "Effects of propellant type on low power arcjet thruster performance", 19th International Symposium on Plasma Chemistry, Bochum, Germany, 2009

[4] Pan W. X., Li T., Huang H. J., et al. "Low power H_2-N_2 arcjet thruster operation and performance", Journal of Propulsion Technology, Vol. 29, No. 4, 2008, pp. 494-498 (in Chinese)

[5] Han P. and Chen X., "Modeling of the supersonic flow and heat transfer in a DC arc plasma torch", Plasma Chemistry and Plasma Processing, Vol. 21, No. 2, 2001, pp. 249–264

[6] Chen Xi, Heat Transfer and Fluid Flow under Thermal Plasma Conditions, Beijing, Science Press. Chapter 3 (in Chinese), 2009

[7] Zhu J., FAST-2D: "A Computer Program for Numerical Simulation of Two-Dimensional Incompressible Flows with Complex Boundaries", Institute for Hydromechanics, University of Karlsruhe, Report No. 690, 1991

[8] Aithal S. M., Subramaniam V.V., "Effects of arc attachment on arcjet flows", AIAA paper, 1996-3295, ASME, SAE, and ASEE, Joint Propulsion Conference and Exhibit, 32nd, Lake Buena Vista, FL, 1996

[9] Babu V., Aithal S.M., and Subramaniam V.V., "Numerical simulation of a hydrogen arcjet", Journal of Propulsion and Power, Vol. 12, No. 6, 1996, pp. 1114-1122

[10] Boyd I. D., "Monte Carlo Simulation of nonequilibrium flow in low power hydrogen arcjets", Paper AIAA-96-2022, the 27th AIAA Fluid Dynamics Conference, New Orleans, Louisiana, 1996

[11] Butler G. W., Boyd I. D., and Cappelli M. A., "Non-equilibrium flow phenomena in low power hydrogen arcjets", AIAA paper, 1995-2819, 31st AIAA/ASME/SAE/ASEE Joint Propulsion Conference and Exhibit, San Diego, California, 1995

[12] Walker Q. E., Characterization and Novel Applications of the Helium Arcjet, PhD thesis, Stanford University, 2007